C.P. No. 1125

C.P. No. 1125

MINISTRY OF TECHNOLOGY

AERONAUTICAL RESEARCH COUNCIL

CURRENT PAPERS

Super VC 10 Cruise Drag- A Wind-Tunnel Investigation

Part I Experimental Techniques

by

C. R. Taylor, J. R. Hall and R. W. Hayward

Aerodynamics Dept., R.A.E., Bedford

LONDON: HER MAJESTY'S STATIONERY OFFICE

1970

PRICE *12s 0d* [*60p*] NET

U.D.C. 533.6.013.12 : 533.6.013.61 : 532.574.27

C.P. No.1125*
August 1969

SUPER VC 10 CRUISE DRAG - A WIND TUNNEL INVESTIGATION (PART I, EXPERIMENTAL TECHNIQUES)

by

C. R. Taylor

J. R. Hall

R. W. Hayward

Aerodynamics Department, R.A.E., Bedford

SUMMARY

Measurements have been made of the longitudinal forces and moments on a 1/27 scale model of the Super VC 10 at Mach numbers between 0.60 and 0.86. This Report gives details of the model design, the test techniques and the corrections applied and includes a critical assessment of measuring techniques used.

---

* Replaces R.A.E. Technical Report 69180 - A.R.C. 31771

CONTENTS

1 INTRODUCTION

This document is the first part of a report on the recent work in the 8ft × 8ft tunnel at R.A.E. Bedford on a 1/27 scale model of the British Aircraft Corporation type 1150 aircraft (the B.O.A.C. variant of the Super VC 10). The main purpose of this work was to produce accurate drag information for a realistic aerodynamic representation of the aircraft at the highest practicable Reynolds number. It is hoped that these measurements, and the subsequent comparison with flight data, will be of value, not only in their specific relevance to the VC 10, but also in providing bases for evaluations of current methods of estimating the cruise drag of subsonic transport aircraft and of wind-tunnel techniques of drag measurement.

This part of the Report is essentially a preamble to the presentation of the results and the analysis, it gives details of the design of the model, the test techniques used and the corrections applied. It also includes a critical assessment of the techniques for accurate drag measurement currently used in the 8ft × 8ft tunnel which could be of interest to anyone concerned with the production and use of model drag data.

The type 1150 Super VC 10 is a long range civil transport aircraft powered by four Rolls-Royce Conway 43D engines. It has a gross weight of 335 000 lb: some dimensions are listed in Table 1. A typical cruise condition for the aircraft is $M_o = 0.80$, $C_L = 0.45$ with the cg at 0.30 $\bar{c}$; at this condition $R_{\bar{c}} \doteq 38 \times 10^6$.

2 BASIC MEASUREMENTS

2.1 Test programme

The basic single-sting tests were made at a Reynolds number of 6 million per foot giving $R_{\bar{c}} = 4.45 \times 10^6$. The Mach number range was from 0.60 to 0.86 (see Table 2 for full details). The model was tested both erect and inverted (see section 2.3) and whenever possible the incidence range covered α ($\bar{C}_L = 0$) to α ($\bar{C}_L = 0.5$) in steps of 0.15 degree.

Additional tests were made (a) to measure the effects of the transition trips (see section 3.3), (b) (using a twin-sting support) to measure the single-sting interference (see section 3.4) and (c) to measure nacelle afterbody pressures and tailplane normal force.

For all the tests the tunnel flow was choked using the variable throat diffuser[1].

2.2 Description of the model

The model was designed and made between February and December, 1965. In order to reduce manufacturing time extensive use was made of existing patterns and patterns cast from an existing 1/27 scale model.

The wings were made, in one piece, from high grade (S97) steel. The wing shape (Fig.2) was defined by ordinates at wing stations 0, 89, 179, 240, 476, 677 and 760 but additional ordinates for stations 20, 60 and 120 were calculated by Lagrangian interpolation between stations 0, 89 and 179. Linear generation was assumed between stations 179 and 240, 240 and 476, 476 and 677 and between 677 and 760. The tip shape was defined by ordinates measured on the aircraft lofts. The basic aircraft ordinates were modified to allow for the estimated wing twist at cruise. The wings were profile machined to within 0.01 in, using wooden patterns; the final shape being obtained by hand finishing to templates.

The 'under-belly' and wing-fuselage junction pieces (see Fig.1) were also made of steel using the same techniques as for the wings. The templates for these pieces were made to ordinates obtained from aircraft lofts. The front fuselage and upper centre section were moulded in glass-cloth and resin to a former from the existing model. Provision was made in the nose for mounting a pressure-switch plus transducer assembly for measuring duct pressures and for a model attitude indicator.

Two rear fuselages were made. That for tests of the complete model and wing + body + tail configurations was made in steel with an integral fin. A simpler glass-cloth and resin unit was made for wing + body and wing + body + nacelle tests. Both rear fuselages had provision for a sting shroud or a tail cone (see Fig.4). The patterns for the rear fuselage and tail assembly were obtained from an existing model with the correct dorsal fin added. The tailplane was also made in steel. Provision was made for nominal tail settings of 0, ±0.5 and +1.5 degrees. The tail-fin junction bullet was moulded in glass-cloth and resin.

Inspection of the model has shown that the true tail-setting angles were:-

Nominal setting η_{nom}	degrees	-0.5	0	+0.5	+1.5
True tail setting η_T	degrees	-0.43	+0.095	+0.54	+1.41

The nacelle struts were made in steel, a mould from the existing model being used for the copy-machining with hand finishing to templates made to ordinates. The angular settings of the nacelle struts on the fuselage could be varied by inter-changing the root fixing blocks to give nacelle incidences of 0, 1.5 or 3.0°. The nacelles themselves were made in aluminium alloy, the external lines again being copied from an existing model. The rearward facing surfaces of the 'beaver tails' between the jet exits were omitted in order to increase the nacelle internal flow (see Fig.9). Each nacelle in the starboard assembly was fitted with four exit static-pressure tappings and a central pitot tube. For supplementary tests 10 external static tappings were added to the port nacelles, the locations of these are shown in Fig.9.

The model was fitted with flap-track fairings, the long cambered inner fence at aircraft wing station 95.90 and the short fences at aircraft wing stations 389.78 and 559.8, (see Fig.2).

The surface finish of the model was good (16 micro-inch for the metal parts, with the plastic components filled and painted) and care was taken to avoid surface waviness. The accuracy of those parts which were copied from the existing model or from patterns and not finished to templates is probably not better than ±0.010 in but great care was taken to define the wing and nacelle-strut shapes accurately and these components have been made to within 0.005 in of the ordinates supplied.

Boundary layer transition trips, consisting of 0.125 in wide bands of sparsely distributed ballotini, sieved to lie within 0.0035 to 0.0041 in diameter, and stuck to the surfaces with a thin film of Araldite adhesive, were applied at 5% chord on the wings, fin, tail, bullet, nacelles and struts. A similar band was located 1.50 in from the fuselage nose. There were no bands inside the nacelles.

For single-sting tests a standard $2\frac{1}{4}$ in diameter six-component strain-gauge balance[2] was fixed to the wing centre-section with its centre at 0.0205 $\bar{c}$ and slightly above the moment reference point. The sting for these tests, which is shown in Figs.3 and 4, was made in 80 ton (S99) steel. The balance location and sting design were optimised to give small support interference with adequate sting strength and stiffness (to help achieve accurate incidence control, and avoid high amplification of flow unsteadiness, the static pitch-amplification ratio* was limited to 1.60).

---

*This is the ratio of change of model incidence to change of quadrant angle.

After the main series of tests had been completed the tailplane mounting was modified to incorporate a normal-force balance.

2.3 Data reduction methods

The force reduction programme for these tests takes the initial balance zeros as the average of the pre-run model-erect and model-inverted, zero-incidence, wind-off readings and corrects these zeros for second-order balance interactions[3] (using model weight components deduced from the erect and inverted wind-off readings) and balance temperature changes. The true balance loads are obtained by applying first and second order balance interactions to the factored differences between the readings and the corrected zeros. The true balance loads are then used to determine the support deflections and hence the true model orientation and (using the measured model weights) the model gravity-force components. The aerodynamic forces are obtained by subtracting the gravity-force components from the true balance loads. The corrected values of kinetic pressure, Mach number and free-stream static pressure are computed for each datum point. The drag and pitching moment data are corrected to free-stream static pressure at the model base. The corrections for model distortion, tunnel buoyancy and constraint, transition-trip drag, nacelle internal drag and support interference are applied before tabulation. Details of the derivation of these corrections are given in this, and subsequent, sectons. A complete list of the corrections applied can be found in Table 4.

Considerations of the effects on drag coefficient of errors in balance interactions and support stiffnesses used on the data reduction shows that any error in these quantities should result in differences between the drag coefficients from model erect and model inverted data, when compared at the same lift coefficient. For example, an error in the measurement of the angular setting of the true balance axial force axis, relative to the sting roll axis, will give equal and opposite errors in the reduced C_D at $C_L = 0$ together with an error which is proportional to C_L and independent of model roll attitude. In order to allow for errors due to these sources, the model was tested both erect and inverted and the true inclination of the balance was deduced from a calibration of the balance while it was in the model in the tunnel.

The results from model-erect and model-inverted data, in fact, differ by $\Delta C_D \mp 0.0005\ C_L$. Small though this error is, it cannot be ascribed to plausible errors in the balance interactions or support stiffnesses. It is concluded that it must result from secondary flows in the tunnel stream (the differences in incidence and pitching moment for a given lift are within the experimental

errors for these quantities) and the model-erect data has been corrected to the mean of the erect and inverted results.

The blockage corrections to tunnel speed and static pressure were obtained, using measured changes in wall pressures from the empty-tunnel condition[1], by the method described in Ref.4 (p.530). The ratios of the blockage static pressure correction to the mean static pressure change at the four roof and floor static holes were calculated, for each configuration tested, by linearised theory[11]. The corrected static and kinetic pressures used in the data reduction were values appropriate to a point on the tunnel centre-line, at the axial position of the wing centre of volume. Typical residual axial velocity distributions*, including blockage effects, are shown in Fig.5 (the residual Mach number variation on the wing is negligible).

The tabulated force coefficients are nondimensionalised in the usual way, using the reference dimensions in Table 1.

3 CORRECTIONS TO BASIC MEASUREMENTS

3.1 Tunnel constraint and wing distortion

As explained in section 2.3 the wall constraint corrections to tunnel static and dynamic pressures and to Mach numbers are calculated by the computer for each datum point and the corrected values are used in the reduction of the results to coefficient form. Small corrections to drag for the pressure gradient due to wake blockage have been applied to the results (see Table 4.1); this correction was evaluated by assuming that the wake images were point sources of strength $D_o/\rho u_o$ where D_o is the configuration profile drag[4].

The boundary induced upwash due to wing lift was calculated by the method of Acum[5]. Thus it was assumed that the spanwise load grading was elliptic but, as has been shown by Bryant and Garner[6], the induced upwash is remarkably insensitive in spanwise loading, and no significant error should arise from this simplification.

To determine the wing distortion under load, the wing was mounted in a special rig and the angles of streamwise twist, at five spanwise stations, due to lift and moment loadings, at each of these stations, were measured. The 'influence-coefficients' so obtained were then used to calculate the wing

---

* Residual Mach number variation is defined as the variation of local effective tunnel Mach number from the corrected Mach number. These variations are due to a combination of empty tunnel and blockage-velocity variations[11].

twist for the calculated lift and moment grading at the datum cruise condition. To obtain the wing twist at other tunnel conditions this basic distribution was scaled in proportion to the model lift (i.e. no allowance was made for variations of C_{LL}/C_L with C_L, M and η_T).

The spanwise variations of boundary-induced upwash and wing distortion at the datum cruise condition ($M_o = 0.8$, $C_L = 0.45$, $R_{\bar{c}} = 4.45 \times 10^6$) are shown in Fig.6. This figure also shows the total incidence variation and the mean correction (see also Table 4.2); the resulting distortion of the wing load grading is compared with the cruise grading in Fig.7. The weighting function used to determine the mean incidence correction is the load grading due to incidence for the wing in reverse flow[7].

The corrections to pitching moment for the total wing incidence variation were calculated by method (iii), equations (3.57) - (3.59), of Ref.7. The correction to drag was based on equation (3.56) of the same reference and hence no allowance was made for the distortion of the load grading on the induced drag.

In calculating the lift-induced upwash the contributions from the tail and nacelle lifts have been ignored. At the cruise condition these effects are truly negligible and at zero model lift the error in tabulated incidence due to these contributions is approximately 0.01°.

The variations of boundary-induced upwash along the tunnel centre-line, relative to corrected incidence, are shown in Fig.8. It can be seen that in each case there is significant curvature of the flow; corrections for this will be deduced in the analysis of the results.

3.2 Nacelle internal flow and jet interference

The external lines of the model nacelles followed those of the aircraft except that the rearward-facing surfaces of the 'beaver-tails' between the jet exits were not reproduced (see Fig.9). The modification to the jet exit region resulted in a 50% increase in exit area (and hence a similar increase in intake flow). The internal surfaces of the nacelles were designed to give smooth convergent ducts. No transition trips were put inside the nacelles and calculations of the boundary-layer growth on the walls of the ducts indicated that the boundary layers would remain laminar right up to the exits. These calculations were made using the formula for laminar boundary layer growth in axisymmetric compressible flow derived by Rott and Crabtree[8], the velocity

variation along the duct being deduced from the onedimensional velocity-area relationship. The criterion for transition onset was that given by Granville[9].

The static pressure at the exit was measured at four points on the walls of each duct in the starboard nacelle assembly during a run in the twin-sting tests. The mass flow and internal drag[10] were calculated using the mean measured static pressures and the estimated boundary-layer thickness by the method for short ducts in Ref.11. Typical values of mean exit static pressure, nacelle mass flow ratio (i.e. free-stream capture area to cowl highlight area) and internal drag are given in the following table (see also Table 4.4):-

M_n	0.60	0.70	0.80	0.84
$\bar{C}_{p_e}$	+0.201	+0.210	+0.224	+0.235
A_∞/A_H	0.525	0.524	0.521	0.512
$C_{D_{int}}$	-0.00002	-0.00001	+0.00002	0.00000

The low values of internal drag are due to the thrust force from the flow deceleration (typically $\Delta C_D = -0.00006$) cancelling the internal friction drag.

The nacelle mass flow ratio for the aircraft at typical cruising conditions is 0.64*. It is unlikely that there is a significant spillage drag penalty for the slightly lower flow ratio of the model tests.

The direct effect of the engine jets on drag has been estimated by comparing the model nacelle pressures at $M_n = 0.80$ (measured in supplementary tests) with similar measurements on an aircraft. The comparison showed that the hot surfaces of the engine beaver tails (these were not represented on the model) collect about three counts of thrust but the drag of the remaining nacelle surfaces is about half a count more, on the aircraft, than on the model. Hence the correction for direct jet interference is $C_D = -0.00025$; the uncertainty in this correction is about ±0.0005. The effects of the jets on tail lift and hence on trim drag will be considered as part of the flight-tunnel comparison.

The tabulated results have not been corrected for jet interference.

---

* Based on a full-scale highlight area of 1708 in^2 per engine.

3.3 Transition-trip drag

As indicated in section 2 the transition trips consisted of sparse bands of 0.0035 - 0.0041 in diameter ballotini stuck to the model surfaces with a thin film of Araldite adhesive. For the main series of tests the width of the bands was 0.125 in. Earlier tests in the 8ft tunnel on a model of the standard VC 10 [12] had indicated the size of ballotini required, however in those tests a much wider bandwidth had been used and it was felt that some confirmation of the effectiveness of the narrower bands was required. Hence, prior to the main series of tests, the variation of model drag, for a range of Reynolds numbers, was measured and some runs were made using an acenaphthene sublimation transition indicator. Due to the rather long run-up times for the tunnel and the difficulties of providing suitable illumination of the model, we are not able to present conclusive photographic evidence of the effectiveness of the transition trips. However, the measured drag variations with Reynolds numbers were consistent with fixed transition positions for Reynolds numbers above 2.5 millions, thus confirming our positive interpretation of the sublimation runs.

Following the main series of tunnel tests, measurements were made of the effects of varying the width of the transition trips of the wings. This was thought to be the easiest way of obtaining a controlled variation of trip drag. As it was anticipated that the effects of excessive band width might be measurably greater for the wing upper surface than for the lower surface, at the higher lift coefficients, the bandwidths were varied independently:-

Run	Bandwidths -	US	LS
1		0.375 in	0.375 in
2		0.375	0.250
3		0.250	0.250
4		0.125	0.250
5		0.125	0.125

Plots of the measured drag variations with Reynolds number for a Mach number of 0.80 and C_L = 0, 0.3 and 0.45 are presented in Fig.10. The measured total drags have been differenced to give drag increments due to changes in bandwidth on one surface only and hence, by appropriate additions, the total drag increments, from the 0.125 in band configuration, for each surface. As shown in Fig.11, the total roughness drag increments vary linearly with bandwidth squared. This sort of variation is quite different to that obtained in

several investigations of roughness drag on thin wings at supersonic speeds[13], but it is known that, for transonic flows over swept wings of moderate thickness, thickening of the boundary layer by the transition trip can cause complicated interactions[14,15]. In these tests the combination of the drag of the trip and its interactions on the wing flow has effectively produced a drag variation which is proportional to bandwidth squared.

The corrections to the measured drags with the 0.125 in bands were deduced from the extrapolation of the plots in Fig.11 back to zero bandwidth. As can be seen from this figure and Fig.12 the correction to wing drag is very small. The corrections for the bands on the nacelles, tailplane etc. were obtained by factoring the wing correction for $C_L = 0$ according to length of band, any addition due to lift on the nacelles, tailplane etc. being truly negligible. The corrections for transition-trip drag are listed in Table 4.5.

The other effects of reducing the width of the roughness bands from 0.375 in to 0.125 in, at $R_{\bar{c}} = 4.45 \times 10^6$, were (a) to increase lift-curve slope by approximately 1% and (b) to shift the aerodynamic centre 0.005 $\bar{c}$ further aft. No change in C_{mo} or zero-lift incidence could be detected. It was deduced from these results that the corrections for the narrow bands, used in the main series of tests, would be less than the estimated systematic errors (see section 4.1) and hence no corrections have been applied to the measured lift and pitching moment for the effects of the transition trips. However, these investigations were made at $M = 0.8$ and $C_L < 0.5$ and it is possible that larger changes in lift or trim with alteration to the transition band could occur at more extreme conditions of M and C_L.

3.4 Sting-support interference

Earlier work in connection with a short-range subsonic transport with rear-mounted engines and a high tailplane had shown that a conventional single-sting support could have significant effects on the lift, drag and pitching moment of the model. The effect on drag depends on the balance between the thrust due to the forward pressure field of the sting, the loss of friction drag on the tail cone and the drag due to the loss of the high pressure region at the fuselage tail and is not amenable to calculation.

Although it was thought that the single-sting support for the VC 10 model would have small drag interference, a separate series of tests was made to measure the support interference. For these tests the model was split at

aircraft station 1250, the wings and front fuselage being mounted on widely spaced twin-stings with the rear fuselage assembly attached to the front part via a strain-gauge balance (see Figs.13 and 14). The gap at the fuselage split was approximately 0.025 in and the vertical alignment at the split was maintained, under conditions of varying rear-fuselage loading, by a small actuator which rotated the rear fuselage about the pivot shown in Fig.14. The pressure in the split cavity was measured by a capsule manometer with a resolution equivalent to $C_D = \pm 10^{-5}$. The 'incidence' of the forward fuselage was measured with a remote reading attitude indicator (essentially a strain-gauged pendulum).

For each of five basic configurations two runs were made using the twin-sting rig (see Table 3). In the series 30 tests the model had the true aircraft rear-fuselage shape and in the series 40 tests the single-sting test geometry was reproduced by fitting the sting shroud to the model and attaching a dummy single-sting to the twin-sting yoke (see Fig.13). Due to flexibility of the twin-sting rig in the heaving mode, it was necessary to articulate the dummy sting so that the correct alignment of the sting in the shroud could be maintained, by remote control of an actuator in the dummy sting. The pressure in the sting shroud was measured in exactly the same way as in the single-sting tests. For each configuration the rear-fuselage loads were corrected to free-stream static pressure in the split cavity and in the sting shroud (if present). The support corrections were then deduced from the changes in rear-fuselage forces, due to the presence of the support, at constant rear-fuselage incidence.

The success of this method of measuring support interference depends (a) on the rear fuselage loads varying only slowly with incidence and (b) on the changes on rear fuselage geometry being small enough to produce no significant effects forward of the split and only small changes in rear-fuselage load. A typical set of results from these tests is plotted in Fig.15.

A complete set of the derived support corrections is given in Table 4.

4 ACCURACY OF RESULTS

4.1 Estimated accuracy of tabulated data

The system for the measurement of model loads which is used in the 8ft tunnel is based on a proven design of compact strain-gauge balance[2] coupled to modified Speedomax potentiometric recorders. By careful calibration of the

balance for first and second order interactions[3] and for temperature effects and by careful control of balance temperature and humidity[11] it has been found possible to obtain axial-force measurements which are repeatable and consistent to within 0.125 lbf. This means that the potential accuracy of the drag measurements in the Super VC 10 model is $\Delta C_D = 0.00005$. The extent to which this potential accuracy can be realised in any test depends mainly on the degree of control of balance temperature and humidity actually obtained, on the steadiness of the model and on the accuracy of the incidence measurement. In the present tests good control of temperature and humidity was obtained and, due to the high support stiffness and the steadiness of the flow which resulted from choking the tunnel flow, the model was particularly steady.

The random errors in the results are extremely small and the indications are that the full potential accuracy of axial force measurement was achieved - witness the consistency in the transition trip drag data at Reynolds numbers near the main test value of $R_c = 4.45$ m. The main errors in the tabulation data are, therefore, the systematic errors.

A detailed assessment of the magnitude of possible systematic errors, due to plausible uncertainties in balance zeros, model weight measurement, base, static and kinetic pressure measurements, incidence and flow direction and also sting interference corrections, has shown that the systematic errors, for each configuration, at a given Mach number, should be within the ranges:-

$$\Delta\alpha = \pm 0.01^\circ$$

$$\Delta C_L = \pm 0.003$$

$$\Delta C_m = \pm 0.005$$

$$\Delta C_D = \pm 0.0001 \pm 0.0002\ C_L \quad .$$

In addition there may be constant systematic errors for the tests as a whole of:-

$$\Delta\alpha = \pm 0.05\ C_L \text{ degrees}$$

$$\Delta C_L = \pm 0.003\ C_L$$

$$\Delta C_m = \pm 0.003\ C_m \pm 0.005\ C_L$$

$$\Delta C_D = \pm 0.00015 \pm 0.0005\ C_L^2$$

these are due to possible inaccuracies in the balance calibration and in tunnel constraint and transition-trip drag corrections.

4.2 Assessment of techniques

The corrected results from the tests described here will be presented in part two of the report which, for commercial security reasons, will have a limited circulation. The assessment of the techniques of measurement and of data reduction and correction could be of more general interest and is therefore included here.

Firstly, we conclude that the tests have demonstrated the feasibility of making accurate subsonic drag measurements at high cruising lift coefficients and at high Reynolds numbers in the 8ft × 8ft tunnel. We believe that the high level of accuracy of the measurements is due to:-

(1) the high degree of flow steadiness which results from choking the tunnel,

(2) the good control of tunnel stagnation temperature (and hence of internal-strain-gauge-balance temperature),

(3) the very careful calibration and alignment of the internal strain-gauge balance,

(4) the 'designed-in' low pitch-amplification ratio.

We also conclude that the high accuracy of the basic measurements is difficult to match in the measurements of the support interference and in the evaluation of corrections for tunnel constraint and model distortion.

The basic potential inaccuracy of the sting support corrections arise from the necessity of measuring these as the differences between model forces in two separate tunnel runs. The potential errors in the sting corrections are therefore twice those of the basic measurements, at the same balance load levels. Potential sources of error are in the corrections for base and cavity pressures and in the measurement of incidence with the model on the twin sting support but, with careful design, these may be minimised. For the VC 10 model the single-sting support was designed to have minimal interference and distortion of the flow at the position of the slit and hence, to have minimal changes in pressure distortion inside the cavity and minimal changes in rear-fuselage to forward-fuselage alignment. The use of an actuated rear-fuselage support should have helped maintain constant slit geometry. Similarly the errors in model fuselage incidence should have been reduced by the use of a direct reading incidence meter.

Systematic errors in the basic measurements, and also in sting corrections, arise principally from inaccuracies in balance calibration and alignment and errors in the evaluation of corrected kinetic and static pressures. Again the use of special techniques can minimise these errors. The type of balance normally used in the 8ft × 8ft tunnel is sufficiently stiff for third-order interactions to be negligible but certain second-order interactions are apparent and these, and the first-order interactions, are measured using a special balance calibration rig outside the tunnel. Small misalignments and inelastic movements at balance-to-sting and balance-to-model joints can give significant errors. These can be minimised[11] by determining consistent alignments and interactions from an in-tunnel calibration in which loads, representative of those for the test, are applied directly to the model, as in the present tests.

The accuracy of the empty tunnel calibration[1] was sufficiently high for the empty-tunnel kinetic pressure to be determined to within 0.125% and the model buoyancy-force correction due to pressure gradient to within $\Delta C_D = \pm 10^{-5}$. We believe that for solid-wall tunnels, the method of correcting Mach number, static pressure, kinetic pressure etc. for tunnel constraint, which uses measured changes in wall pressures, is both reliable and accurate. The measured changes in wall pressures have often been observed to be in good agreement with linear-theory predictions and here we are relying on linear theory only for the ratio of blockage-velocity increment to wall-velocity increment, under conditions in which the main uncertainty in the theoretical model (i.e. the wake blockage) is very small. The changes in wall pressure are based on an empty-tunnel calibration of high accuracy and care is taken to preserve the condition of the wall holes. The constancy of the calibration is assured by the cleanness of the tunnel air, the low humidity (0.0001 lb/lb) and the absence of screens.

The residual Mach number variations over the model are very sensitive to free stream Mach number and can lead to inaccuracies at the higher speeds (see Fig.5). In the present case, at $M_o = 0.86$, the kinetic pressure at the tail was approximately 0.6% lower than at the wing, which suggests that the model was, perhaps, too big for tests at that Mach number. This flow speed variation is almost entirely due to fuselage blockage. For a solid-wall tunnel it is approximately proportional to $\ell^4 \beta^{-4} f^2$, where $\beta^2 = 1 - M_o^2$, and f is the ratio of the diameter to the length (ℓ) of the body, and hence may impose serious limits on the accuracy of solid-wall tunnel tests, or on the size of model, at high Mach numbers.

As is mentioned elsewhere, due to the high resolution of the quadrant incidence digitiser, the robustness of the quadrant and the low pitch-amplification ratio of model support, the basic incidence measurement is very accurate. The calculation of wall-induced upwash can, with care, be performed to a compatible accuracy. This is not thought to be sensitive to variations from the assumed loading, at constant lift coefficient. On the other hand, the aeroelastic wing incidence distortion is the difference between bending and twist contributions and this is sensitive to the assumed loading. The effective mean incidence of the distorted wing in the non-uniform boundary-induced upwash field can be determined, for a theoretical inviscid small perturbation flow model, by recourse to a reverse-flow theorem but this cannot be expected to remain valid at the high Mach number, high lift-coefficient conditions of main interest in the present tests and we believe that the uncertainty in corrected incidence arising from this source may be as much as $\pm 0.05°$ C_L. We have similar reservations about the validity of our methods of correcting pitching moment for the residual incidence variation.

The constraint correction to drag which we have used ignored changes in drag due to changes in lift distribution. The error due to this is almost impossible to estimate with any confidence but may not be very significant since we suspect that, at or near cruising conditions, the redistribution of the lift will both increase the vortex drag and decrease the profile drag. With the experience now available future models could be designed to have the correct wing geometry at a prescribed datum test condition.

As mentioned in section 2.3 the differences between the model-erect and model-inverted results are ascribed to variations in tunnel flow direction and the mean of these two sets of data has been quoted in the tabulated results. In principle the true value of drag for a given lift could be less than either erect or inverted values but taking into account the known form of the spanwise loading we conclude that the true drag lies between the two measured values and the quoted values are probably not more than one drag count (0.0001) in error, due to this uncertainty.

We regard the investigation of transition trip effects on drag under cruise conditions as definitive. Although the variation of trip drag shown in Fig.11 might be regarded as unusual, it is the only variation which is consistent with more than 60% of the measurements and it is a plausible one for this model. It is possible that the drag of the wider bands would have varied with Mach number (this was not looked at) but it is felt that the drag of the

narrow bands used for the main body of the tests is sufficiently small for possible variations with Mach number to be ignored. The behaviour of the wider bands at high lift coefficient is not unusual. The apparent increase in roughness drag with Reynolds number is accompanied by an increase in incidence for constant lift coefficient and hence implies an increase in boundary layer thickness on the upper surface due to the excessive width of the roughness band.

One of the most significant possible sources of error arises from the virtual impossibility of providing a representative simulation of engine flows. The approach adopted for the VC 10 tests was the one often used of increasing the nondimensional model intake entry flow to a value near to full scale (or at least high enough to avoid significant spillage drag) by enlarging the duct exits. The exit flows are then completely unrepresentative but, at least for the VC 10, the estimated loss of thrust due to the absence of the jet plume is small.

5 CONCLUSIONS

From the assessment of the techniques of measurement and of data reduction and correction we conclude that, provided sufficient care is taken in setting up the model and calibrating the strain-gauge balance, accurate subsonic drag measurements can be made in the 8ft × 8ft tunnel on models of subsonic transport aircraft at high cruising lift coefficients and high Reynolds numbers. The maximum model size will be determined by the possible uncertainties in the results arising from residual variations in angle of incidence and Mach number, induced by the effects of wall constraint and model distortion. Adequate techniques are available for determining the corrections for model-support interference, provided this can be minimised during model design. The drag of minimum transition trips is within the plausible experimental error.

The present series of tests have provided data of sufficient accuracy for a realistic evaluation of the Super VC 10 drag 'break-down' and an extrapolation to full-scale conditions for comparison with flight measurements.

Table 1

SOME AIRCRAFT AND MODEL DIMENSIONS

		Aircraft		Model
Length		146 ft 8 in		5.4321 ft
Wing span	b	146 ft 2 in		5.4136 ft
*Wing Ref. area	S	2806 ft^2		3.8491 ft^2
*Wing Ref. length	$\bar{c}$	20 ft 0.2 in		0.7414 ft
'Aspect ratio'	b^2/S		7.614	
*Wing $\frac{1}{4}c$ sweepback	outer wing		32.5°	
*Wing t/c	outer wing		9.8%	
Intake highlight area (per engine)		1708 in^2		2.343 in^2

Moment reference point at 0.3 $\bar{c}$

0.0562 $\bar{c}$ above fuselage datum

Base area (*single or dummy sting*) 0.0491 ft^2

*True dimensions for type 1100 wing

Table 2

SINGLE-STING CONFIGURATIONS AND TEST RANGES

Config. No.	Description	Designation	Tailplane incidence η_T	Nacelle incidence η_N	$R_c \times 10^{-6}$	Mach number range
01	Body alone	B			4.45	a except 0.76
02	Wing+Body	W+B			4.45	a
03	Wing+Body+Tail	W+B+T	0.54°		4.45	a
04	Wing+Body+Tail	W+B+T	1.41°		4.45	a except 0.76 and 0.86
05	Wing+Body+Nacelles	W+B+N		3°	4.45	a
06	Complete model*	C	0.54°	3°	4.45	a
07	Complete model*	C	-0.43°	3°	4.45	a
08	Complete model*	C	1.41°	3°	4.45	a
09	Complete model	C	0.54°	1.5°	4.45	a

* including tailplane normal force measurements in supplementary tests.

Mach number range (a):-

Nominal:-	M_n:-	0.60	0.70	0.74	0.76	0.78	0.80	0.82	0.84	0.86
True:-	M_o:-	0.597	0.697	0.738	0.758	0.778	0.797	0.818	0.838	0.859

Table 3

TWIN-STING CONFIGURATIONS AND TEST RANGES

Config. No.		Description	$R_c \times 10^{-6}$	Mach number range
32	AS	02 but with true rear end and no dummy single sting	4.45	b
33		03 " "	4.45	b
35		05 " "	4.45	b
36		06 " "	4.45	b
38		08 " "	4.45	b
42	AS	02 including distorted rear end and dummy single sting	4.45	b
43	AS	03 " "	4.45	b
45	AS	03 " "	4.45	b
46	AS	06 " "	4.45	b
48	AS	08 " "	4.45	b

Mach number range (b):-

Nominal:-	M_n:-	0.60	0.70	0.76	0.80	0.84	0.86
True:-	M_o:-	0.596	0.692	0.752	0.792	0.831	0.845

Table 4

CORRECTIONS APPLIED TO SINGLE-STING RESULTS

1 Buoyancy corrections

(i) Empty tunnel static buoyancy $10^4 \Delta C_D$

M_n:-	0.60	0.70	0.74	0.76	0.78	0.80	0.82	0.84	0.86
Config.									
01	0.3	0.5	0.4	0.3	0.2	0.2	0.2	0.1	-0.2
02	0.3	0.6	0.5	0.3	0.2	0.2	0.2	0.1	-0.3
03-04	0.5	1.0	0.9	0.7	0.6	0.6	0.5	0.4	-0.1
05	0.4	0.8	0.7	0.5	0.2	0.2	0.2	0.1	-0.3
06-09	0.5	1.2	1.1	0.9	0.6	0.6	0.6	0.4	-0.1

(ii) Wake buoyancy $-10^4 \Delta C_D$

M_n:-	0.60	0.70	0.74	0.76	0.78	0.80	0.82	0.84	0.86
Config.									
01	0.1	0.2	0.2	0.2	0.2	0.2	0.3	0.3	0.4
02	0.3	0.4	0.5	0.5	0.6	0.6	0.7	0.8	1.0
03-04	0.4	0.5	0.6	0.7	0.7	0.8	0.9	1.1	1.3
05	0.3	0.4	0.5	0.5	0.6	0.7	0.8	0.9	1.0
06-09	0.4	0.6	0.7	0.8	0.9	1.0	1.1	1.2	1.5

2 Wall constraint corrections

(i) Config. 01

All constraint corrections are zero.

(ii) Configs. 02-09

M_n:-	0.60	0.70	0.74	0.76	0.78	0.80	0.82	0.84	0.86
$\Delta\alpha/C_L$:-	0.38°	0.36°	0.35°	→	→	→	→	→	→
$\Delta C_D/C_L^2$:-	+0.0092	→	→	→	→	→	→	→	→
$\Delta C_M/C_L$	-0.0030	-0.0040	-0.0042	-0.0044	-0.0045	-0.0047	-0.0050	-0.0050	-0.0050

Table 4 (Contd.)

3 Flow distortion corrections

$\Delta C_L = 0$

$\Delta C_M = 0$

$10^3 \Delta C_D/C_L$

M_n:-	0.60	0.70	0.74	0.76	0.78	0.80	0.82	0.84	0.86
Config.									
03-04 06-09	-0.30	-0.40	-0.45	-0.50	-0.55	-0.60	-0.65	-0.70	-0.80
01, 02, 05	-0.30	-0.30	-0.30	-0.30	-0.35	-0.45	-0.50	-0.60	-0.65

4 Nacelle internal drag corrections (Standard internal drag[10] corrections)

For configurations 05-09 only

M_n:-	0.60	0.70	0.74	0.76	0.78	0.80	0.82	0.84	0.86
$10^4 \Delta C_D$	+0.2	+0.1	+0.1	+0.1	-0.1	-0.2	-0.2	0.0	+0.1

5 Transition trip drag corrections

For all Mach numbers

Config.	$10^4 \Delta C_D$	$\Delta C_D/C_L^2$
01	-0.0	0
02	-0.7	-0.00030
03-04	-1.2	-0.00030
05	-0.9	-0.00030
06-09	-1.3	-0.00030

6 Single sting support corrections

Correction to C_L applied as ΔC_L

Correction to C_M applied as ΔC_M

Correction to C_D applied as $\Delta C_D + K C_L$

Table 4 (Contd.)

Config.	ΔC_L	ΔC_M	ΔC_D				K
M_n :-	All	All	0.6-0.8	0.82	0.84	0.86	
01	0	0	-0.00018	→	→	→	0
02	-0.001	+0.002	-0.00018	→	→	→	-0.00008
03-04	-0.004	+0.013	+0.00024	→	→	→	-0.00060
05	+0.003	-0.006	-0.00019	-0.00016	-0.00009	+0.00004	+0.00028
06-09	-0.002	+0.010	+0.00015	+0.00016	+0.00020	+0.00026	0

SYMBOLS

A_∞	nacelle free-stream capture area
A_H	nacelle intake highlight area
b	wing span
c	local wing chord
$\bar{c}$	reference length - standard mean chord
C_D	drag coefficient
$C_{D_{int}}$	internal drag coefficient
C_L	overall lift coefficient
$\bar{C}_L$	wing lift coefficient (including wing-induced lift on body)
C_{LL}	section lift coefficient
C_m	overall pitching moment coefficient
$\bar{C}_{p_e}$	nacelle-exit static-pressure coefficient
M_o	corrected Mach number
M_n	nominal Mach number
q	free-stream kinetic pressure
$R_{\bar{c}}$	free-stream Reynolds number, based on $\bar{c}$
S	reference area
α	fuselage incidence
β	$\sqrt{1 - M^2}$
η_T	tailplane setting, relative to fuselage centre-line
η_N	nacelle setting, relative to fuselage centre-line

REFERENCES

No.	Author(s)	Title, etc.
1	D. Isaacs	Calibration of the 8ft × 8ft wind tunnel at subsonic speeds. A.R.C. R.& M. 3583 (1967)
2	G.F. Moss D.G. Payne	A compact design of six-component internal strain gauge balance. R.A.E. Technical Note Aero 2764 (1961)
3	T.A. Cook	A note on the calibration of strain gauge balances for wind tunnel models. R.A.E. Technical Note Aero 2631 (1959)
4	L. Howarth (Editor)	Modern development in fluid dynamics, high speed flow. Vol.II (pp.530-531) Oxford (1953)
5	W.E.A. Acum	Corrections for symmetrical swept and tapered wings in rectangular wind tunnels. A.R.C. R.& M. 2777 (1950)
6	L.W. Bryant H.C. Garner	Control testing in wind tunnels. A.R.C. R.& M. 2881 (1951)
7	H.C. Garner	Lift interference on three-dimensional wings. Chapter III of Agardograph 109 (1967)
8	N. Rott L.F. Crabtree	Simplified laminar boundary-layer calculations for bodies of revolution and for yawed wings. Jour. Aero. Sci. Vol.19, No.8, pp.553-565, August 1952
9	P.S. Granville	The calculation of the viscous drag of bodies of revolution. D.T.M.B. Report 849, July 1953
10		Report of the definitions panel on the thrust of a jet engine and of the internal drag of a ducted body. A.R.C. C.P. 190 (1954)
11	C.R. Taylor J.R. Hall	Techniques for the accurate measurement of drag in subsonic wind-tunnels. R.A.E. paper to be published
12	G.F. Moss	R.A.E. paper to be published

REFERENCES (Contd.)

No.	Author(s)	Title, etc.
13	J.Y.G. Evans	Transition fixing techniques and the interpretation of boundary-layer conditions on slender wings in supersonic wind tunnels. R.A.E. Technical Note 2946 (A.R.C. 25892) (1964)
14	J.A. Blackwell	Effects of Reynolds number and boundary-layer transition location on shock-induced separation. Agard C.P. 35
15	H.H. Pearcey J. Osborne A.B. Haines	The interactions between local effects at the shock and rear separation - source of significant scale effects in wind-tunnel tests on aerofoils and wings. Agard C.P. 35

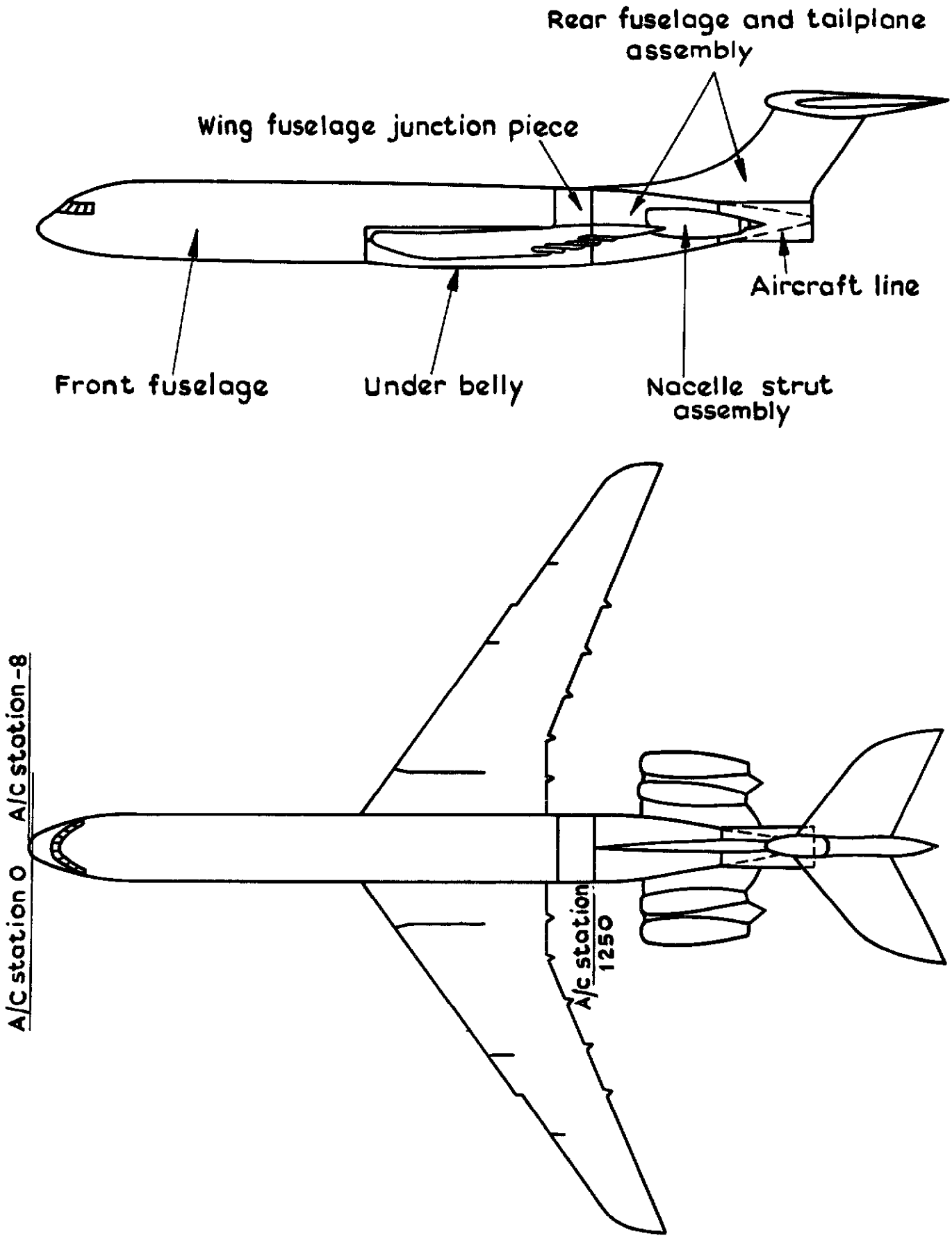

Fig.1 General arrangement of model

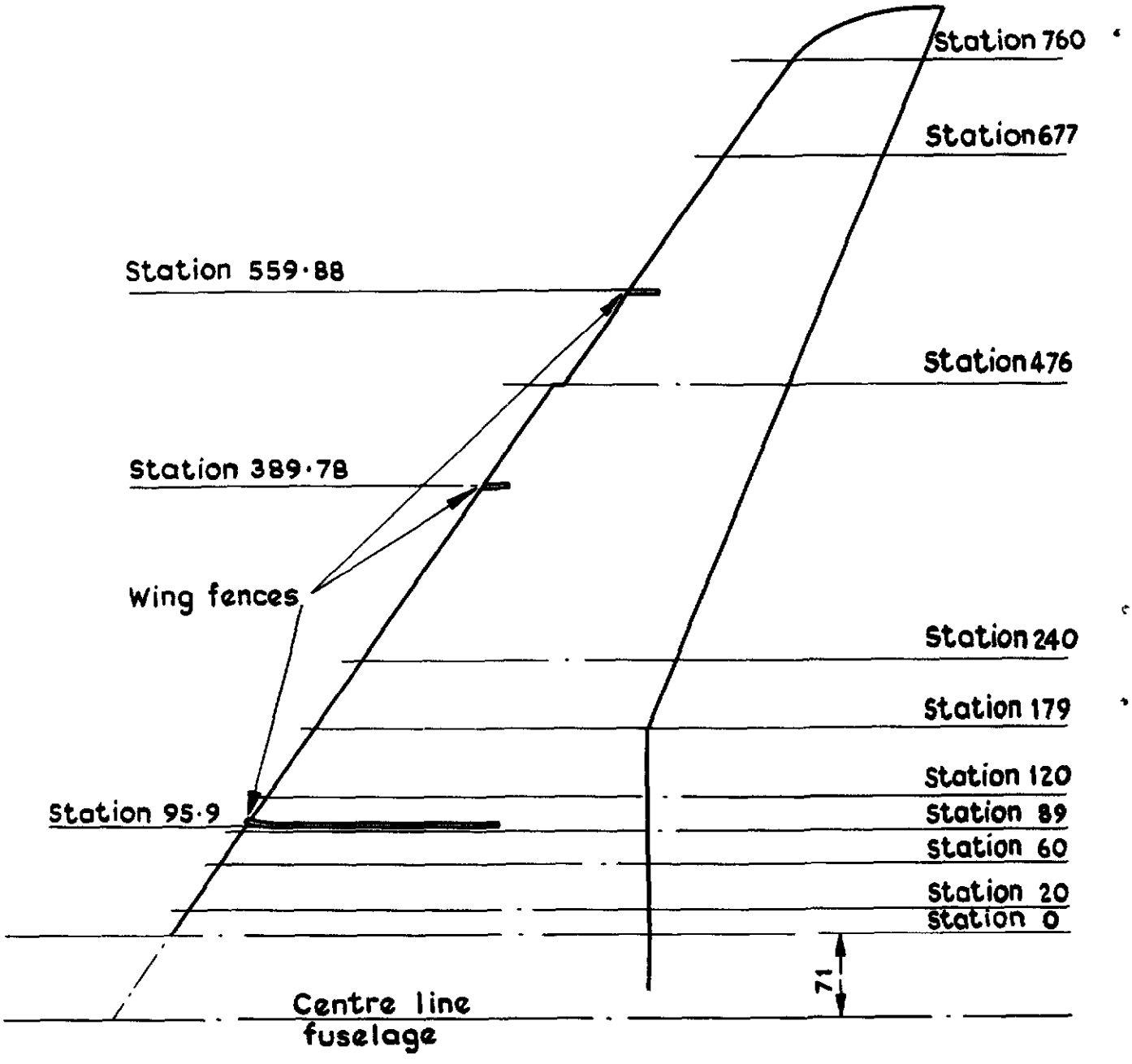

Fig.2 Details of wing

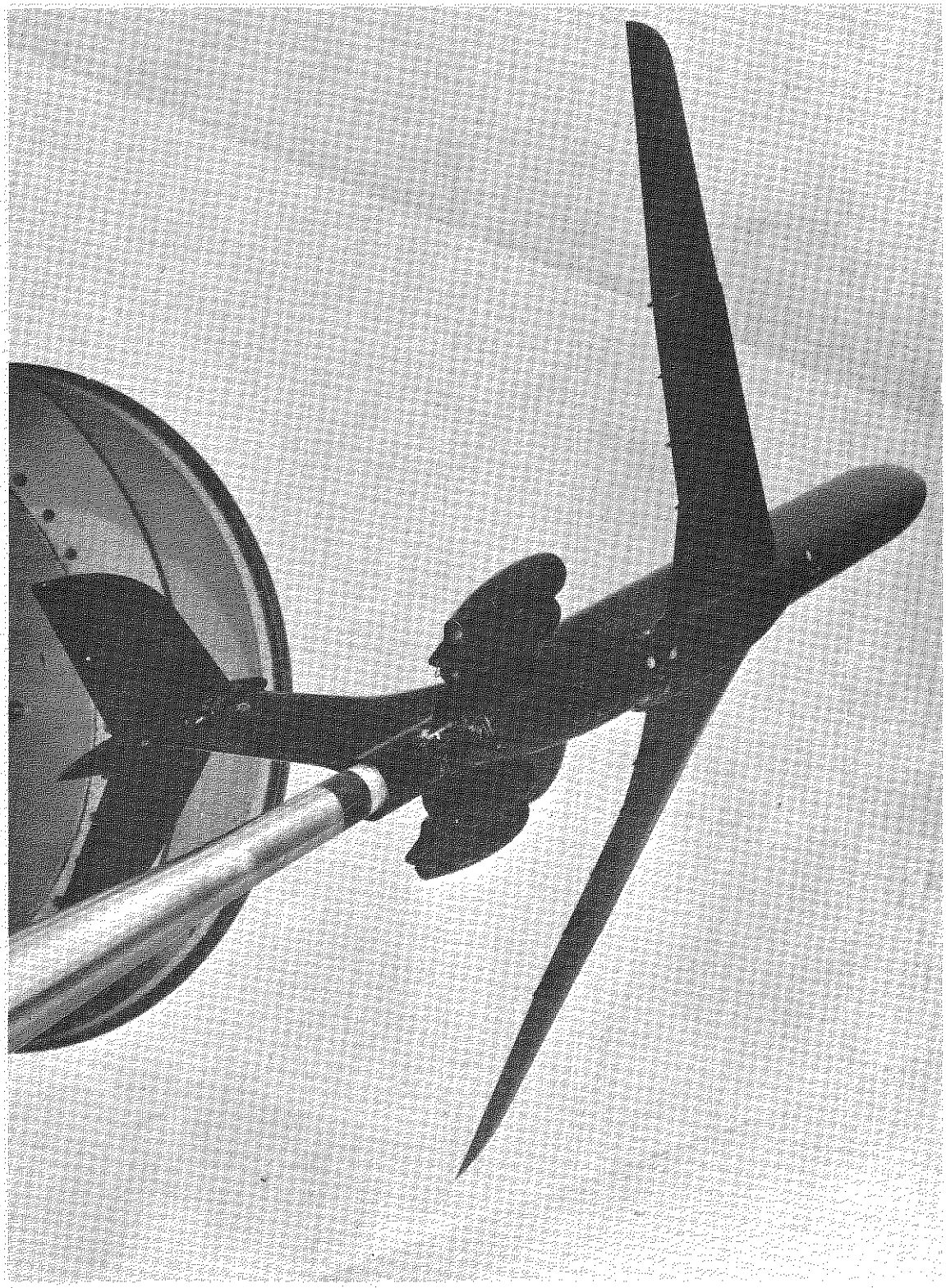

Fig 3. Model on single-sting support

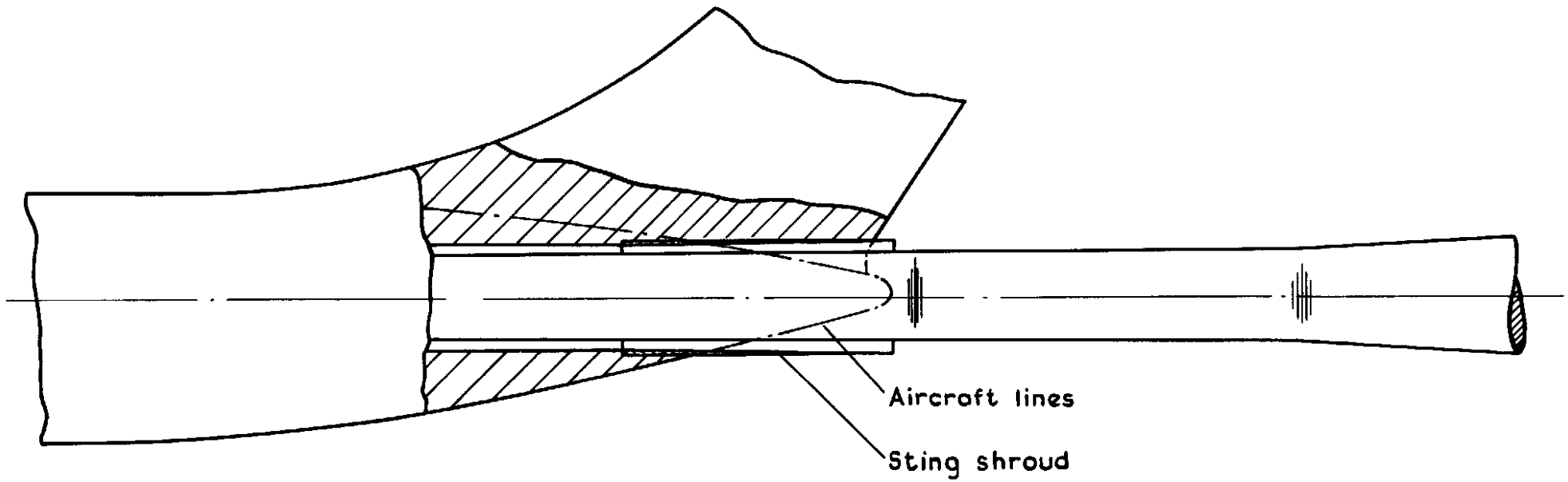

Fig.4 Model on single sting support, rear fuselage and sting geometry

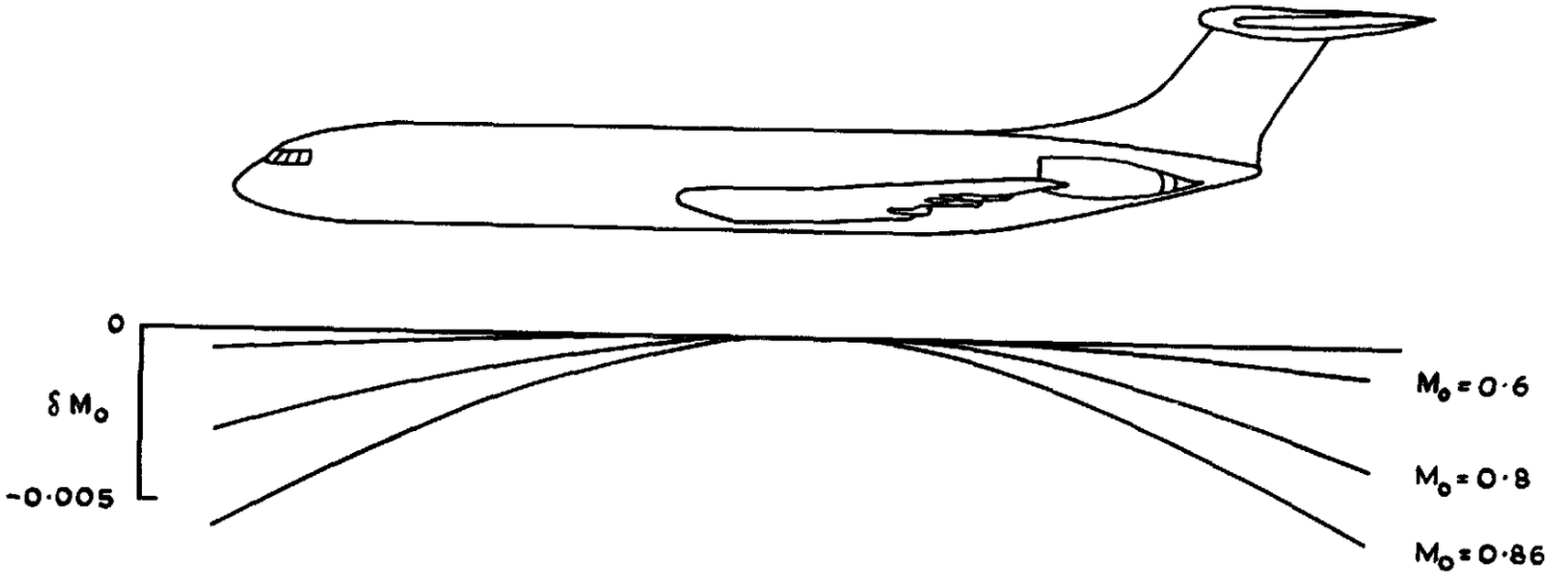

Fig.5 Residual Mach number variation along model

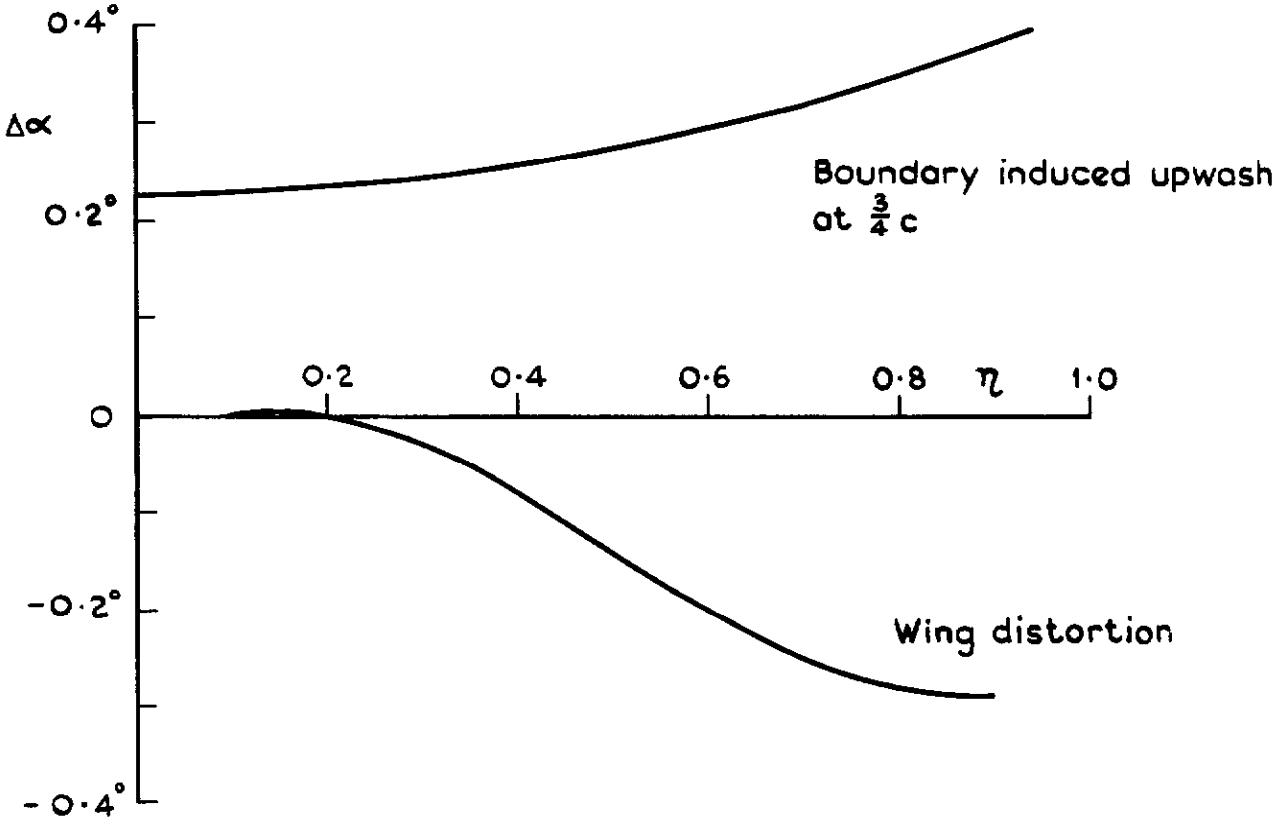

a Boundary-induced upwash and wing distortion

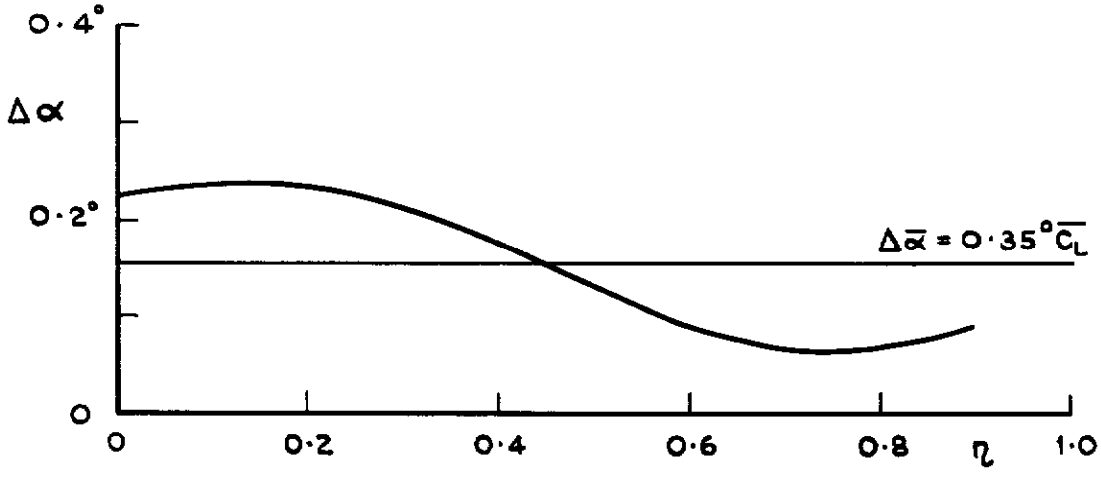

b Total variation and mean correction

Fig.6a&b Spanwise variations of boundary-induced upwash and wing distortion
($M_o = 0{\cdot}8$. $\bar{C}_L = 0{\cdot}45$, $R_{\bar{c}} = 4{\cdot}45$ m)

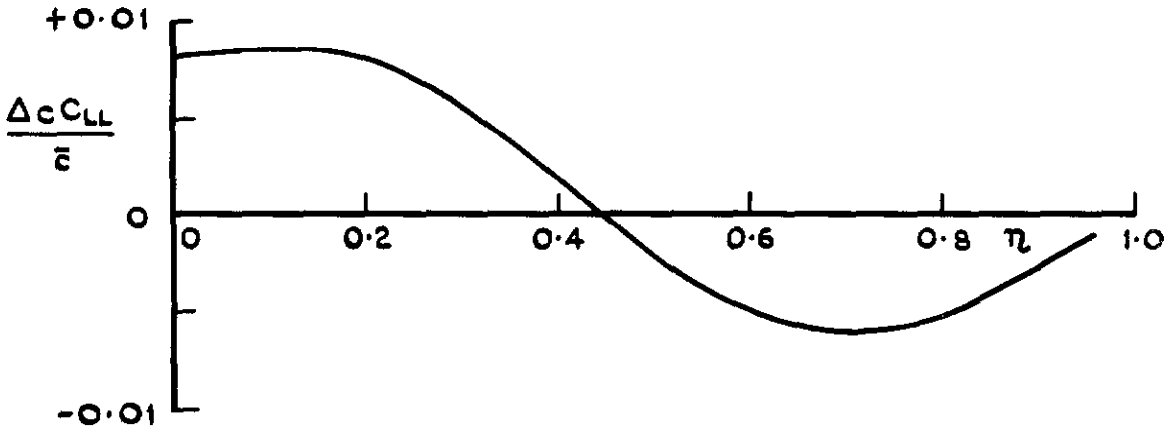

a Distortion of wing load grading

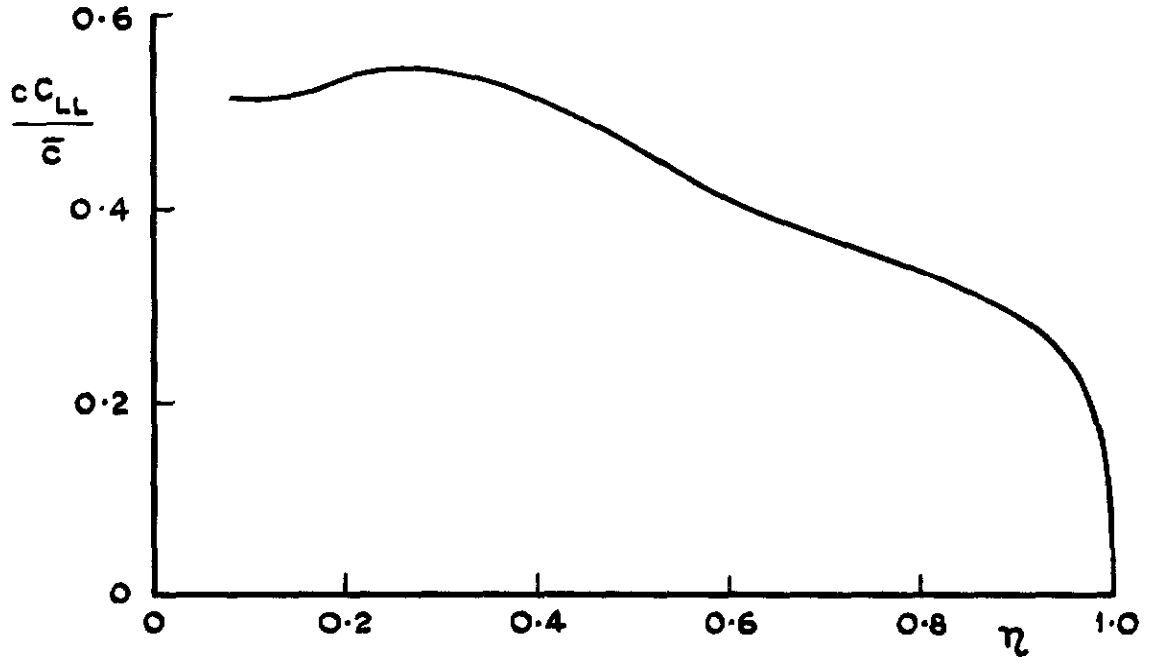

b Estimated aircraft load grading

Fig.7a &b Distortion and estimated cruise wing load gradings
($M_o = 0·8$, $\bar{C}_L = 0·45$, $R\bar{c} = 4·45m$)

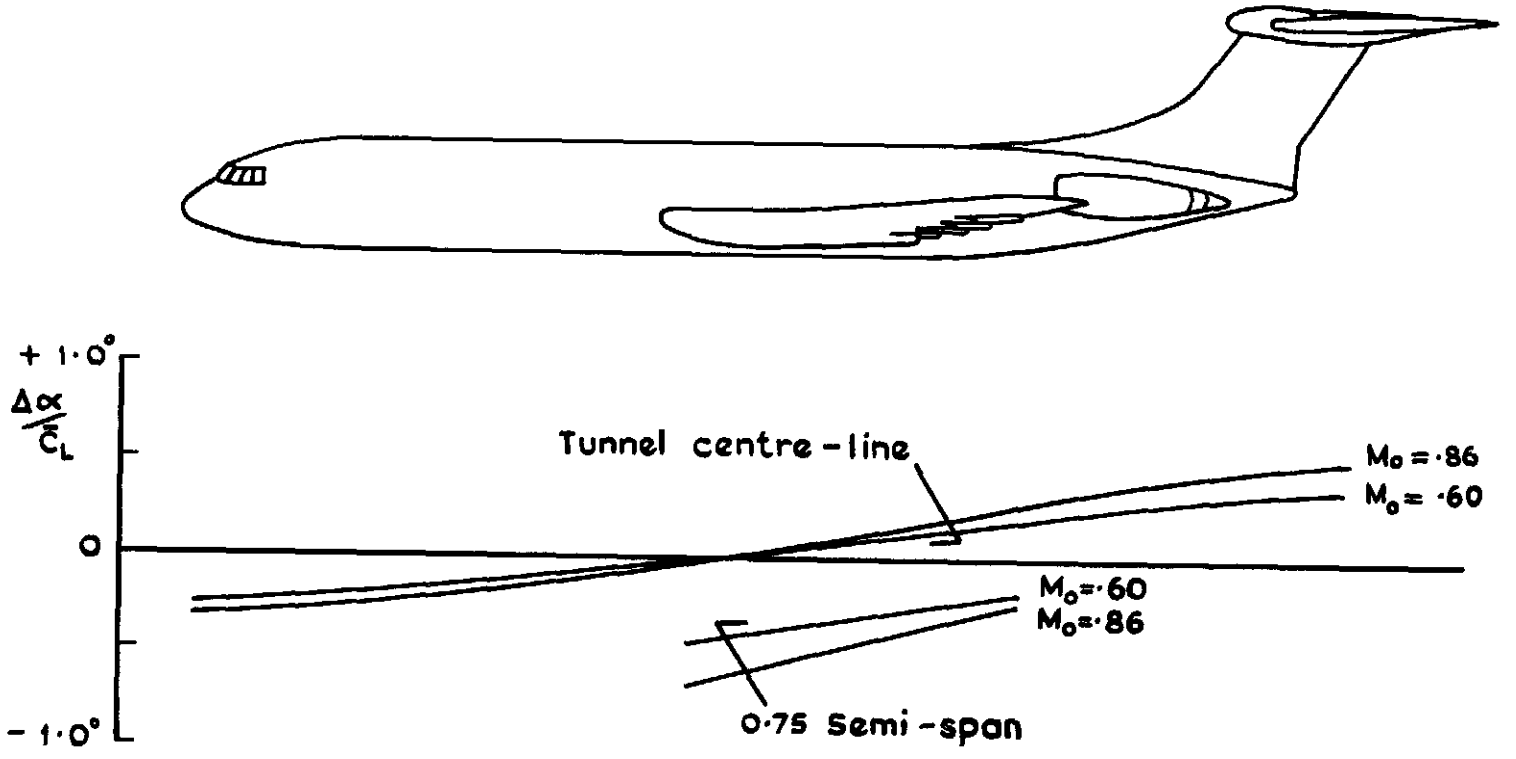

Fig.8 Residual incidence variation along the model

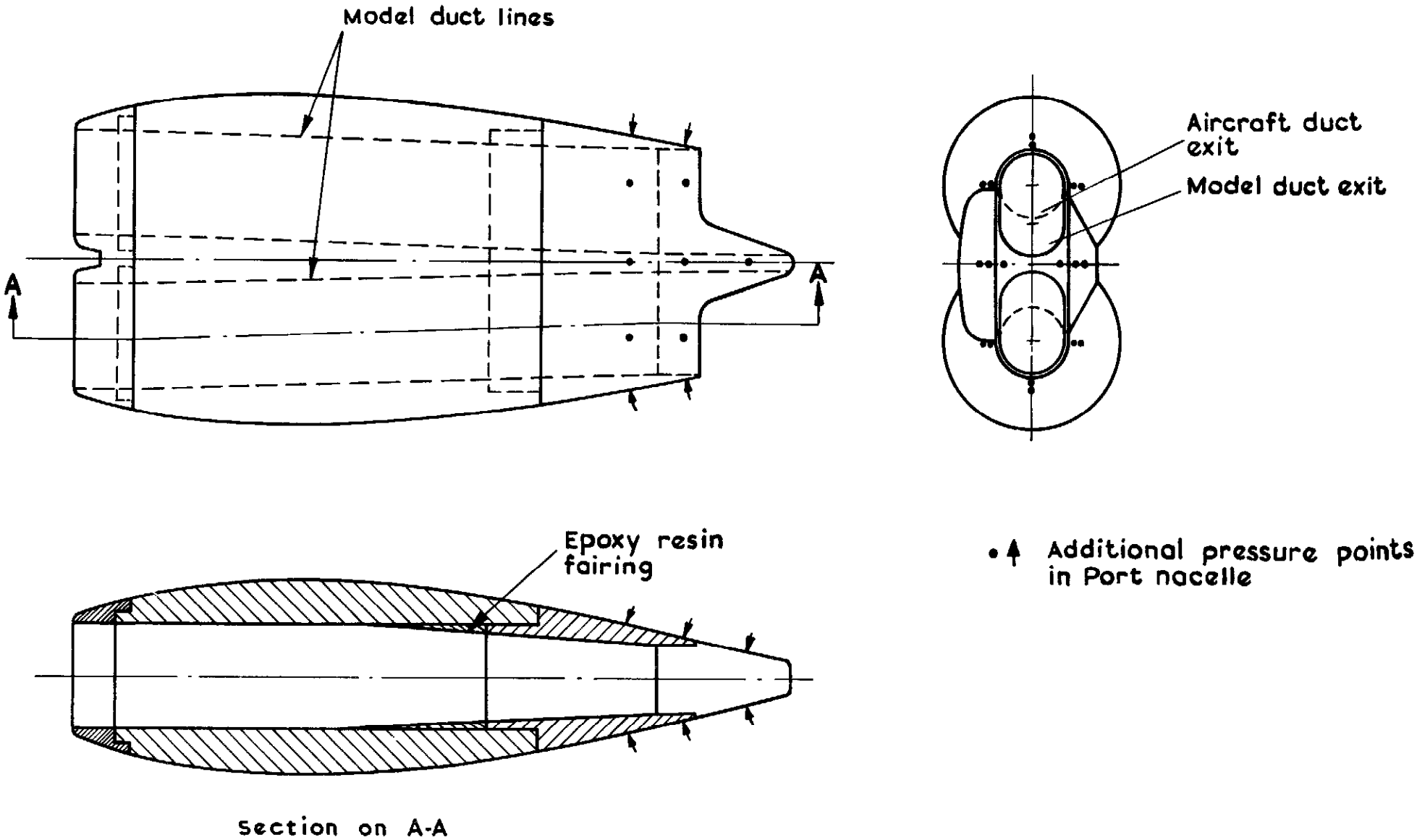

Fig.9 Model nacelle geometry

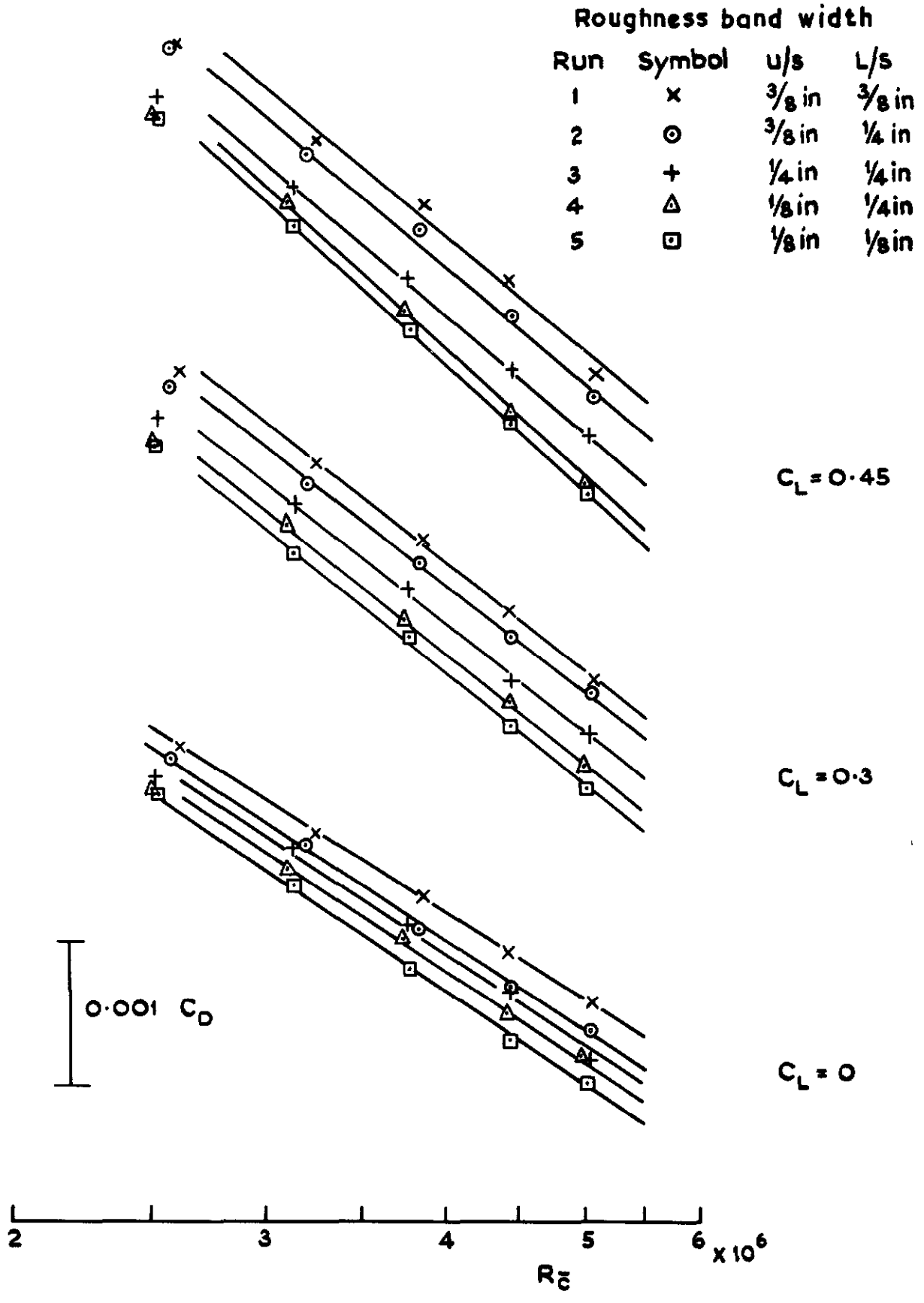

Fig.10 C_D v $R\bar{c}$ at $M_n = 0.8$ for various roughness bands

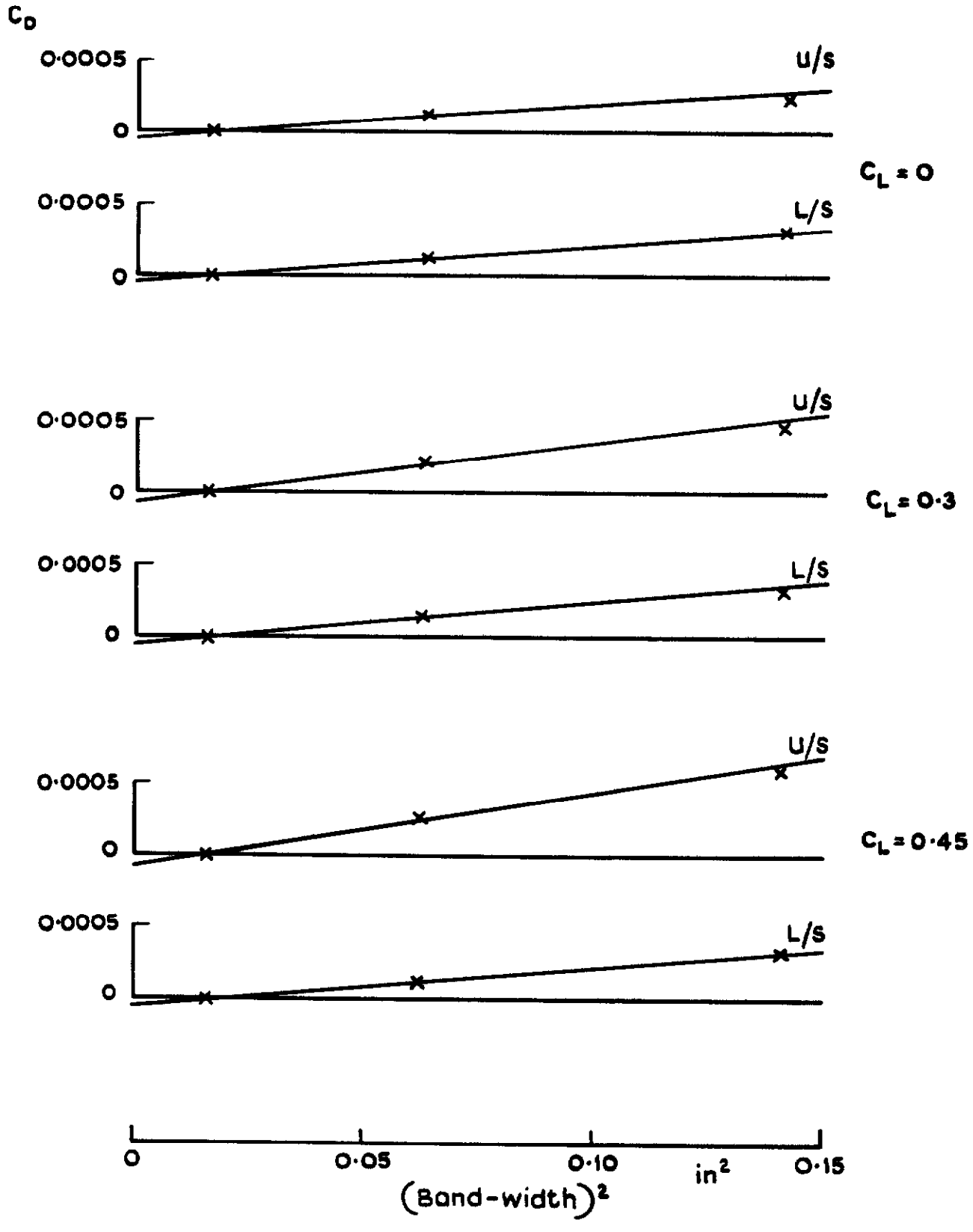

Fig.11 Variation of wing roughness drag with band width
$M_n = 0·8$, $R\bar{c} = 4·45m$

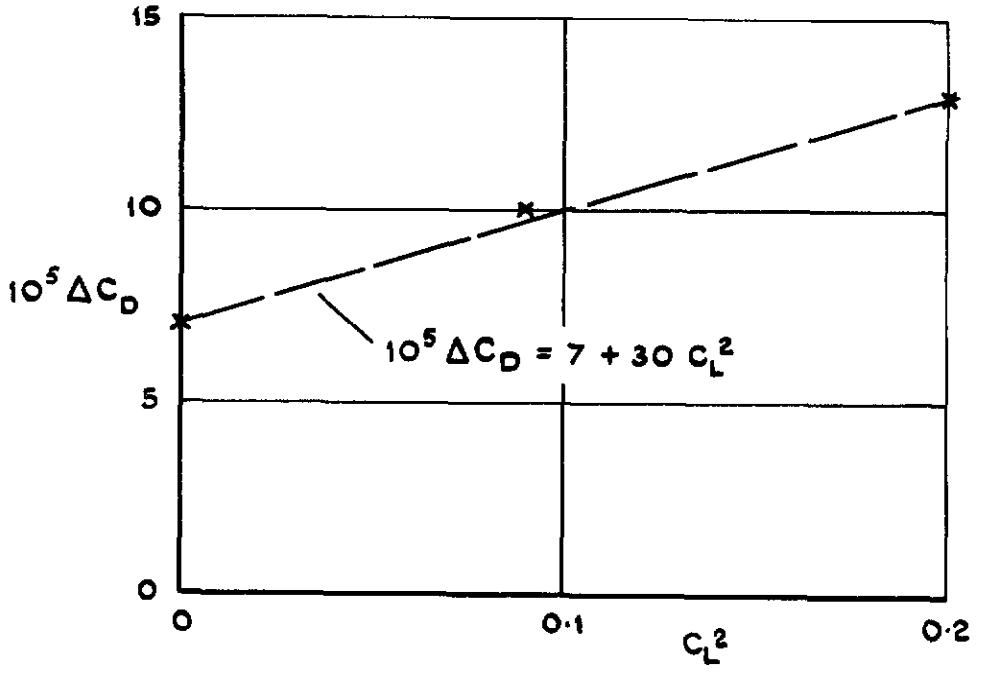

Fig.12 Derived wing roughness drag

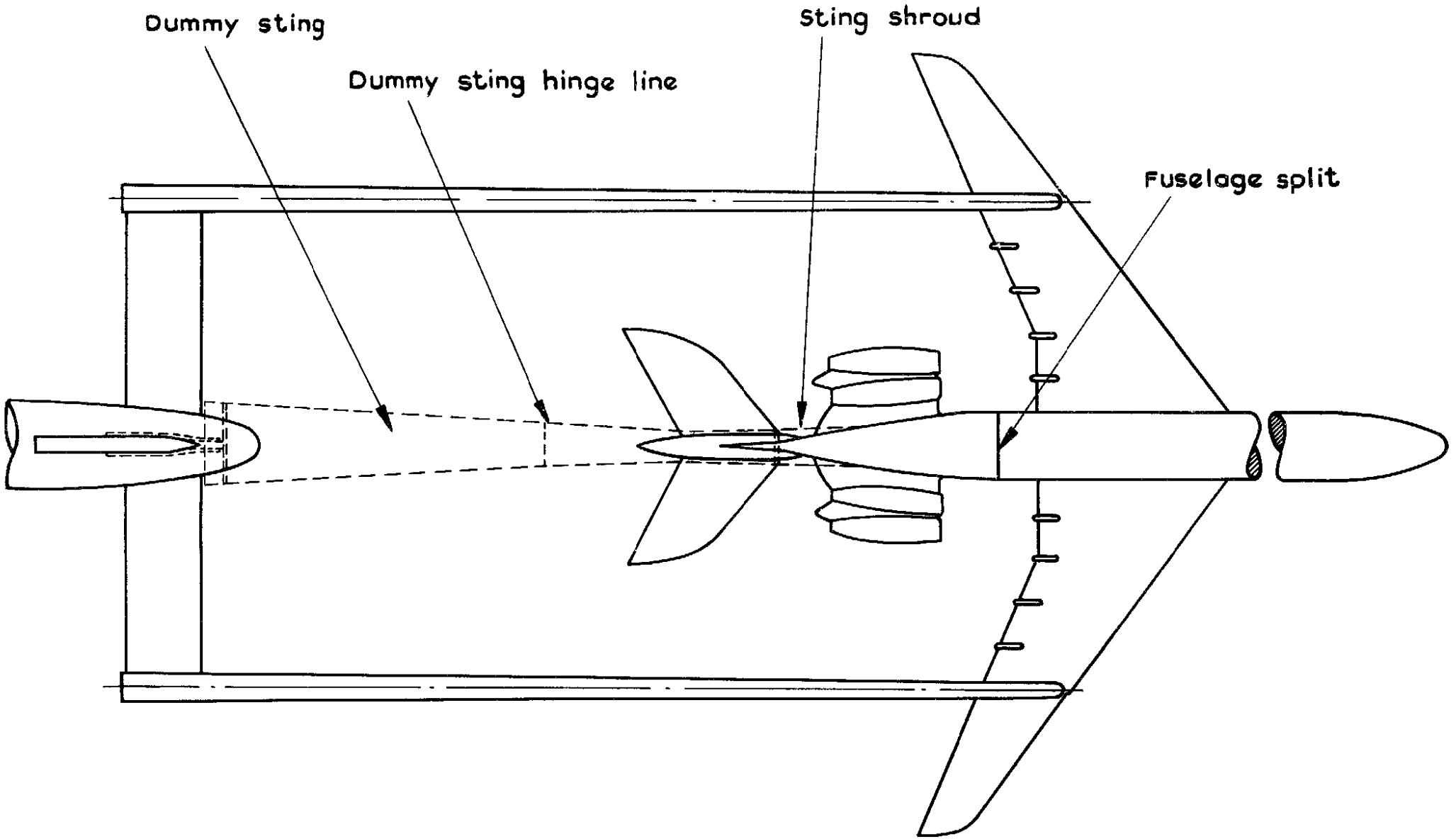

Fig.13 Model on twin sting support

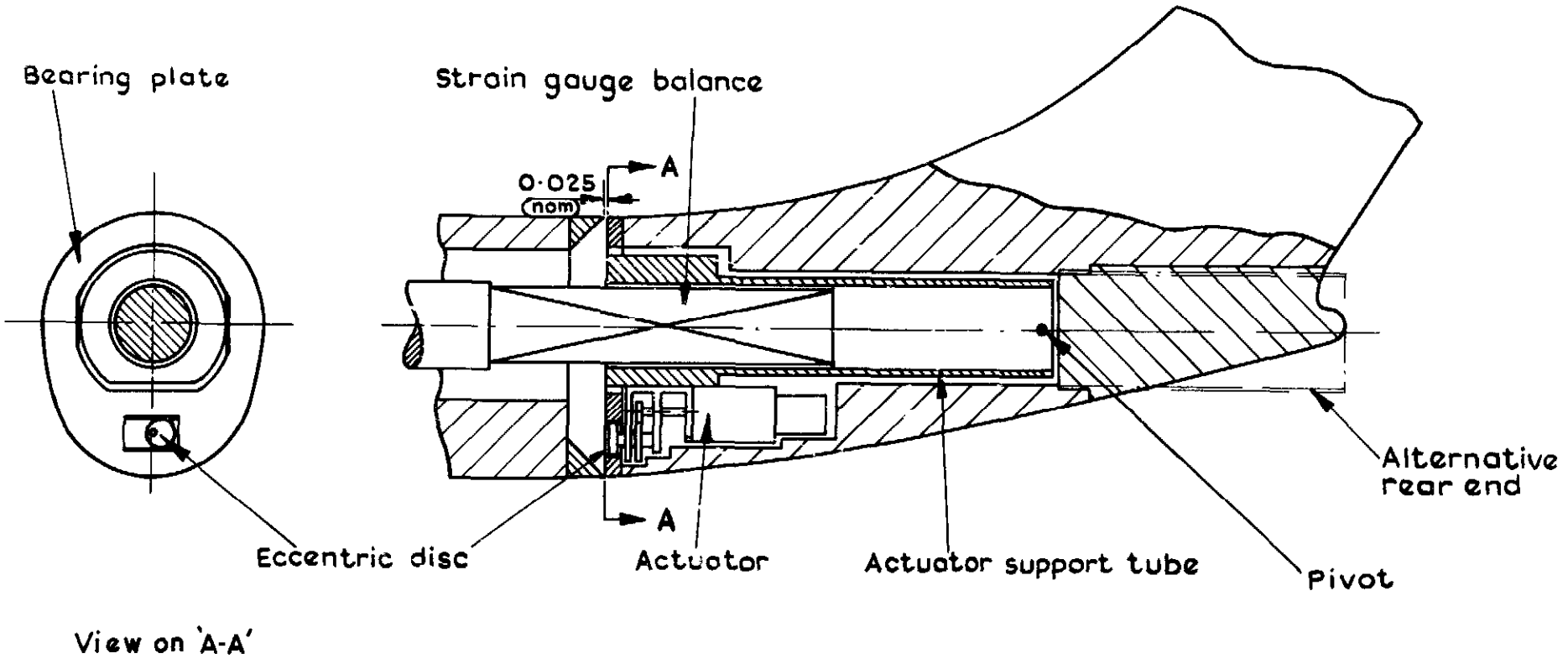

Fig.14 Rear-fuselage assembly for twin-sting test

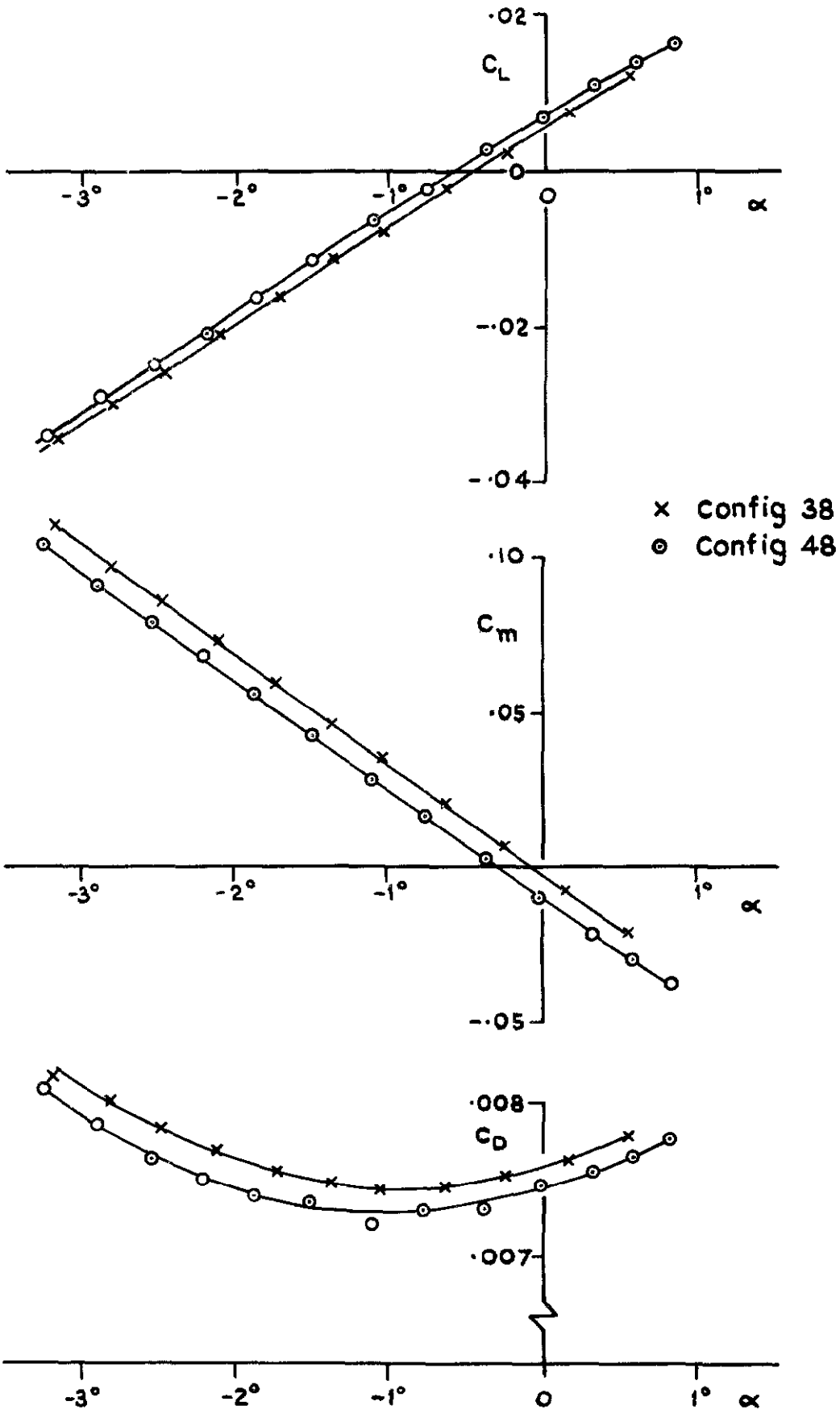

Fig.15 Typical results from twin-sting runs. $M_n = 0{\cdot}8$

Printed in England for Her Majesty's Stationery Office by the Royal Aircraft Establishment, Farnborough Dd 501371 K 4.

DETACHABLE ABSTRACT CARD

A.R.C. C.P. No.1125
August 1969

533.6.013.12 :
533.6.013.61 :
532.574.27

Taylor, C. R.
Hall, J. R.
Hayward, R. W.

SUPER VC 10 CRUISE DRAG - A WIND TUNNEL INVESTIGATION
(PART I, EXPERIMENTAL TECHNIQUES)

Measurements have been made of the longitudinal forces and moments on a 1/27 scale model of the Super VC 10 at Mach numbers between 0.60 and 0.86. This Report gives details of the model design, the test techniques and the corrections applied and includes a critical assessment of measuring techniques used.

A.R.C. C.P. No.1125
August 1969

533.6.013.12 :
533.6.013.61 :
532.574.27

Taylor, C. R.
Hall, J. R.
Hayward, R. W.

SUPER VC 10 CRUISE DRAG - A WIND TUNNEL INVESTIGATION
(PART I, EXPERIMENTAL TECHNIQUES)

Measurements have been made of the longitudinal forces and moments on a 1/27 scale model of the Super VC 10 at Mach numbers between 0.60 and 0.86. This Report gives details of the model design, the test techniques and the corrections applied and includes a critical assessment of measuring techniques used.

Published by
HER MAJESTY'S STATIONERY OFFICE

To be purchased from
49 High Holborn, London W.C 1
13a Castle Street, Edinburgh EH 2 3AR
109 St Mary Street, Cardiff CF1 1JW
Brazennose Street, Manchester 2
50 Fairfax Street, Bristol BS1 3DE
258 Broad Street, Birmingham 1
7 Linenhall Street, Belfast BT2 8AY
or through any bookseller

C.P. No. 1125

SBN 11 470313 2